Analysis of whole slide images of equine tendinopathy

Matthieu Toutain, Olivier Lezoray, Fabrice Audigié, Valeria Busoni, Giacomo Rossi, Francesco Parillo, Abderrahim Elmoataz

Analysis of whole slide images of equine tendinopathy

M. Toutain[1], O. Lézoray[1], F. Audigié[2], V. Busoni[3], G. Rossi[4], F. Parillo[4], and A. Elmoataz[1]

[1] Université de Caen Basse-Normandie, GREYC UMR CNRS 6072, Caen, France
[2] CIRALE, USC INRA BPLC 957, Ecole Nationale Vétérinaire d'Alfort, Goustranville, France
[3] Service d'imagerie, Faculté de Médecine Vétérinaire, Université de Liège, Liège, Belgium
[4] Dipartimento di Scienze Veterinarie, Universita degli Studi di Camerino, Matelica, Italy

Abstract. We present a method for the automatic analysis of whole slide histological images of equine tendinopathy. This computer-aided analysis is a prescreening tool that helps veterinarians doctors to evaluate the efficacy of new treatments. A set of textural, arrangement, and alignment features are extracted to reproduce visual histological criteria, each of them representing different feature views of the initial data. To efficiently combine these different views of the data for clustering, tensor-based multi-view spectral clustering is considered and provides an unsupervised classification of the tissue zones.

1 Introduction

Tendons are dense bands of fibrous connective tissue that act as intermediary in the attachment of muscle to bone. During locomotion, they act as viscoelastic structures submitted to great tensile strength [1]. These biomechanical properties arise from a specific spatial architecture reflecting the requirements of this tissue. The main constituents of tendons are thick, closely packed parallel bundles of longitudinally oriented collagen fibers. Cells, mainly fibroblasts and vessels, are arranged in a healthy tendon in long parallel rows in the spaces between the collagenous bundles [2]. In sport and racing horses, the two flexor tendons of the equine hand (the superficial digital flexor tendon and the deep digital flexor one) are submitted to high forces during the stance phase of the stride. Intense and repeated stresses on these tendons can lead to overstress injuries, from simple tendonitis to rupture. Tendinopathies in sport and racing horses are a major cause of reduced performance and temporary or permanent breakdown of the athletic horse career. Up to 10 to 15% of the horse population is affected by tendinopathies, which represents a major impact of several millions euros a year. Diagnostic imaging (high resolution ultrasonography and magnetic resonance imaging) of these diseases [3] has enabled major diagnosis advances during the last 15 years. Meanwhile, experimental studies have been conducted to validate the efficacy of new therapeutic approaches to improve the healing of injured tendons [4].In such studies, assessment of positive effects of new treatments on the tendon healing process is frequently demonstrated using detailed histological analysis on tendon samples. However these histological analysis are based on either subjective or semi-quantitative analysis performed by an expert operator. Moreover the analysis of the entire slide of the tendon sample is particularly difficult in such an expert-based approach. Consequently, the

purpose of our study is to develop an objective and quantitative method using criteria close to those used by expert operators for analyzing whole histological slides of equine tendon samples. Such an approach may be extremely useful for assessing objectively, with a non-operator dependent method, the efficacy of new tendon treatments.

2 Unsupervised analysis of equine tendon samples

Whole slides of Hematoxylin-Eosin (HE) stained equine tendon samples were scanned at $40\times$ magnification using a ScanScope CS^{TM}(Aperio$^{®}$, San Diego, CA) digital microscopical scanner. To facilitate visualization and processing, scanned samples are directly stored as a multi-resolution image [5] where each level of resolution is an under-resolved version of the highest resolution image. The image being very large (40000×30000 at the highest resolution), each resolution level is split into image tiles (of size 512×512) in a non-overlapping layout. We take advantage of this tiled multi-resolution organization in our approach to analyzing the tendon samples. First, the lowest resolution image is processed to discriminate tissue versus background. The corresponding partition enables to retain, at the highest resolution, only tiles that contain tissue. Second, on the retained tiles, cells are extracted according to their color. Third, for each high-resolution tile, three different feature vectors are computed to reproduce visual histological criteria used to quantify tendon injury (texture, arrangement and alignment of the cells). Fourth, having tiles described by three different sets of features, a tensor-based multi-view spectral clustering is considered to discriminate the different tissue areas.

2.1 Tissue segmentation

Scanned samples contain two main elements at the lowest resolution: tendon tissue and slide background. The tendon tissue can be easily discriminated from background on the lowest resolution picture (Figure 1). Following the strategy developed in our previous works [5], the tiles of the lowest resolution image are processed in the following way. Each tile is simplified by weighted Laplacian regularization and a 3D color histogram is constructed from the RGB color vectors of all the tiles. This histogram is clustered with a 2-means classification (see in [5] for details and motivations on this whole strategy). This extraction of the tissue performs extremely fast and well, but some small tissue regions as well as holes in the segmented tissue still remain (both artifacts being due to the tendon cutting). To cope with this, we use a morphological hole filling followed by an opening by reconstruction. Figure 1 presents two results of tissue extraction on healthy and injured tendon samples. The detection of the tissue is projected on the highest level of resolution and this enables to determine the high-resolution tiles containing tissue. Only these tiles are further considered for analysis.

2.2 Extraction of cells

Several histological visual criteria assessment of equine tendinopathy rely on the shape, the arrangement, and the alignment of cells. Therefore, to be able to derive quantita-

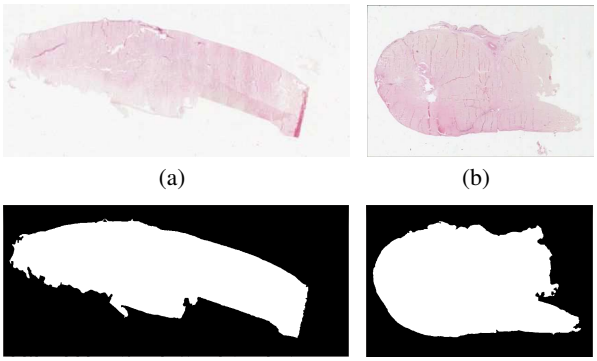

Fig. 1. (a) Transverse healthy superficial digital flexor tendon sample, (b) Transverse injured deep digital flexor tendon sample, (c)-(d) Segmented tissues of samples (a)-(b).

tive measures for these visual criteria, cells have to be extracted in the retained high-resolution tiles inside the tissue region. To extract cells, since the coloration of slides is known (Hematoxylin-Eosin), we can separate the individual dyes. According to the Beer-Lambert law, the transmission of incident light $\mathbf{I}_0$ through a specimen can be modeled as $\mathbf{I} = \mathbf{I}_0 e^{-\mathbf{SX}}$ where $\mathbf{I}$ is the incident light after passing through the specimen, $\mathbf{S}$ the absorption factors of the dyes and $\mathbf{X}$ their concentrations. This can be reformulated in terms of optical density: $\mathbf{Od} = -\log(\frac{\mathbf{I}}{\mathbf{I}_0}) = \mathbf{SX}$. The optical density of each RGB channel is linear with the amount of dye and can be used, given the absorption factors $\mathbf{S}$, to extract the amounts of dyes $\mathbf{X}$ in a specimen. To achieve correct balancing of the absorption factors for separate dyes, the columns of $\mathbf{S}$ are normalized to unit length. Then, we obtain $\mathbf{X} = \mathbf{S}^{-1}\mathbf{Od}$. This whole process is often called color deconvolution [6]. To summarize, we convert vectors $\mathbf{f}$ from the RGB color space to vectors $\mathbf{h}$ in a new color space comprising hematoxylin, eosin, and background channels with $\mathbf{h} = \mathbf{S}^{-1} \times -\log(\frac{\mathbf{f}}{\|\mathbf{f}\|})$. For the absorption factors, we used values from [6] and retain only the hematoxylin channel since this dye stains cells in blue (in our preparation of the samples, the dye is applied longer than necessary to saturate the staining). The extracted hematoxylin channel is then binarized using an automated thresholding. Figure 2 shows the segmentation of cells superimposed an initial sample image corresponding to four adjacent high-resolution tiles.

2.3 Feature Extraction

Once cells have been extracted in all the high-resolution tiles, we are in position of extracting features to describe the content of each tile with respect to histological visual criteria assessment of equine tendinopathy. Many visual criteria are used by pathologists to quantify tendinopathy, one can quote, e.g., alignment, arrangement and crimp of collagen fibers, density and shape of cells, neovascularization intensity, etc. In this

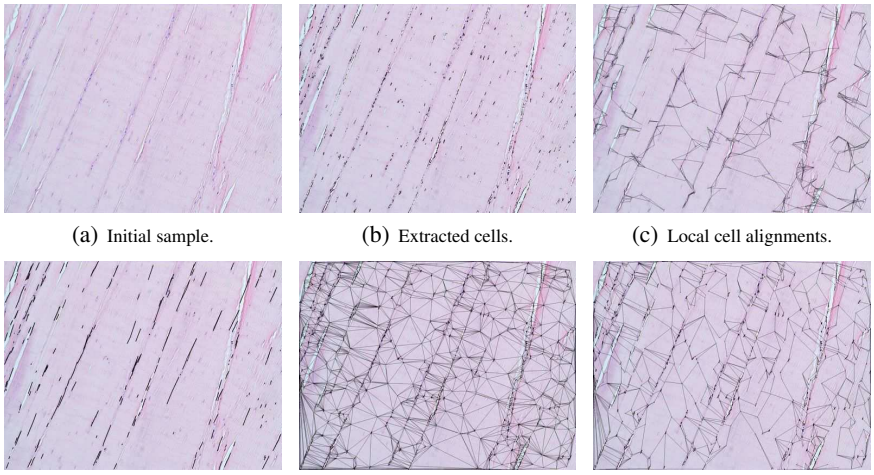

(a) Initial sample. (b) Extracted cells. (c) Local cell alignments.

(d) Global cell alignments. (e) Delaunay triangulation. (f) Minimum Spanning Tree.

Fig. 2. (a) a longitudinal healthy superficial flexor tendon sample, (b) extracted cells, (c) locally detected alignments, (d) globally detected alignments, (e)-(f) Delaunay triangulation and MST.

paper, we have chosen to extract textural, arrangement and alignment features to quantify the different areas in the tendon tissue.

Textural features Texture is more regular when the tissue is healthy than when the tissue is injured. We chose here to describe texture with uniform gray-scale and rotation invariant Local Binary Patterns [7] in 3×3 squares. From this LBP pattern, an LBP histogram is constructed for each tile of the highest resolution image. From these histograms, an $N \times N$ distance matrix denoted $\mathbf{W}^{(1)}$ is computed between all the tiles of the image (N being the number of tiles) with the χ^2 distance measure : $d_H(h_1, h_2) = \sum_{i=1}^{N} \frac{[h_1(i)-h_2(i)]^2}{h_1(i)+h_2(i)}$ with h_1 and h_2 two histograms to compare.

Arrangement features From the extracted cells, it is important to quantify their architecture as well as density and shape. These visual features relate to neighboring properties of the cells and can be quantified using graph based techniques [8]. To use graphs, the m cell centroids $c^1, c^2, ..., c^m$ in the whole slide are considered as graph vertices. From this set of vertices, specific graphs are computed on the *whole slide*. Figure 2 illustrates the graphs we consider. Then, for each tile, a normalized arrangement feature vector is computed from the corresponding sub-graphs. With these arrangement feature vectors, an $N \times N$ distance matrix denoted $\mathbf{W}^{(2)}$ is computed between the tiles with the Euclidean distance. Features are computed as detailed below.

Voronoi Diagram - The Voronoi diagram V is composed of a set of polygons $P = \{P_1, P_2, \cdots, P_m\}$. Any centroid c is included in polygon P_a if $d(c, c^a) = \min_j\{\|c -$

$c^j \|\}$ where $a, j \in \{1, 2, ..., m\}$ and $\|c - d\|$ is the Euclidean distance between any two centroids c, d. We calculate the areas of all $P \in V$, and the average and disorder are calculated for areas of all P, giving two feature values.

Delaunay Triangulation - The Delaunay graph D is constructed such that any two unique centroids c^a and c^b, where $a, b \in \{1, 2, ..., m\}$, are connected by an edge $E^{a,b}$ if P_a and P_b share a side in V. We calculate the sides lengths for all triangles in D, and take the average, disorder, and maximum of these to obtain three feature values.

Minimum spanning tree - Given a connected, undirected graph, a spanning tree S of that graph is a subgraph that connects all its m vertices with $m - 1$ edges. Weights w_S^E are assigned to each edge E in each S based on the length of E in S. The sum of all weights w_S^E in each S is determined to give the weight $\hat{w}_S$ assigned to each S. The minimum spanning tree (MST) denoted by S' has a weight $\hat{w}_S^{'}$ less than or equal to $\hat{w}_S$ for every other spanning tree S. We calculate the average and disorder of the branch lengths in S' to obtain two features values.

Nuclear features - The shape of cells is also a criterion of arrangement. The shape descriptor we consider is the elongation of cells. This criteria is a major parameter in the analysis of the cell type and of its functional activity (active versus quiescent fibroblasts particularly). We calculate average and disorder of elongation values to obtain two feature values.

Alignment features Cell alignment is also a very important histological feature that describes properties of collagen fibers. To detect alignments of cells, we adapted the approach proposed in [9]. Let $A = \{a_1, ..., a_n\}$ be a group of points in $\mathbb{R}^2$. A is aligned iff there exists an angle $\theta \in [0, \pi)$ where for all pairs of points a_i and $a_j (i \neq j)$, a_j is in the direction θ or $\theta + \pi$ of a_i, relatively to the horizontal axis. From the set of cell centroids on the *whole slide*, a nearest neighbor graph G is constructed, and weighted with the angle between two points and the horizontal axis. The dual graph $\tilde{G}$ is then obtained and weighted with the difference between two edges of G. The dual graph $\tilde{G}$ represents all the alignment distances (in the chosen neighborhood) between two pairs of points (a_i, a_j) and (a_j, a_k). The dual graph is pruned in order to keep only locally aligned sets of vertices. Therefore, only edges with a weight lower than an alignment detection threshold β are preserved: $\tilde{G}_{TH} = (\tilde{V}, \tilde{E}_{TH})$ with $\tilde{E}_{TH} = \{(i, j) \in E | \tilde{e}_{ij} < \beta\}$. The connected components $\mathfrak{C}_k$ of $\tilde{G}_{TH}$ correspond to locally aligned groups of vertices (Figure 2(c)) that are a possible candidates for being globally aligned groups of vertices. To detect this, if the maximum weight (representing the degree of global alignment) of $\mathfrak{C}_k$ is higher than β, the vertex of maximum degree (the less aligned one) is suppressed and we repeat this until $\mathfrak{C}_k$ is globally aligned (under the constraint of containing at least 3 vertices). With the result of the algorithm (Figure 2(d)), we create an histogram of the angles of the detected alignments for each tile in the highest resolution image. As previously, with these histograms, an $N \times N$ distance matrix denoted $\mathbf{W}^{(3)}$ is computed between all the tiles with the χ^2 distance measure.

2.4 Tensor-based multi-view spectral clustering

In the feature extraction step, textural, arrangement, and alignment feature vectors were extracted to describe tiles of the tendon tissue region. These feature vectors represent different views of the data that provide complimentary informations to each-other. In this paper, we consider a spectral clustering of the data based on some similarity measure between the data. With multiple views, we have multiple similarity matrices, and we want to perform a (spectral) clustering based on the combined representation of similarities. This is known as a multiple-view approach to clustering [10]. Multi-view spectral clustering can be formalized as the following optimization problem:

$$\max_{\mathbf{U}} \sum_{i=1}^{K} ||\mathbf{U}^T \mathbf{S}_N^{(i)} \mathbf{U}||_F^2, \text{ s.t. } \mathbf{U}^T\mathbf{U} = \mathbf{I}. \tag{1}$$

where K is the number of different views of the data (i.e., the number of similarity matrices), $\mathbf{S}_N^{(i)}$ is a normalized similarity matrix for the i^{th} view constructed from the $\mathbf{W}^{(i)}$ distance matrices, and $\mathbf{U}$ is the common factor matrix shared by the different views. Since the similarity of each view is computed in different spaces, the normalization of each similarity matrix is required. Classical single view spectral clustering is recovered for $K = 1$. A tensor $\mathcal{X} \in \mathbb{R}^{N\times N\times 3}$ is build from these three similarity matrices $\{\mathbf{S}_N^{(1)}, \mathbf{S}_N^{(2)}, \mathbf{S}_N^{(3)}\}$. Multi-linear singular value decomposition (MLSVD) [11], is a form of higher-order extension of matrix singular value decomposition. It decomposes a tensor $\mathcal{X}$ into a tensor $\mathcal{C}$ multiplied by a matrix along each mode. Tensor $\mathcal{C}$, known as the core tensor, is analogous to the diagonal singular value matrix in conventional matrix SVD. The matrices of each mode are called factor matrices and can be considered as a PCA of the tensor along each mode. This leads to the following (Tucker) decomposition: $\mathcal{X} = \mathcal{C} \times_1 \mathbf{U}_1 \times_2 \mathbf{U}_2 \times \mathbf{U}_3$ where $\mathbf{U}_1, \mathbf{U}_2 \in \mathbb{R}^{N\times N}$ and $\mathbf{U}_3 \in \mathbb{R}^{K\times K}$ and $\times_n$ is the mode-n product [11]. Given a tensor $\mathcal{X}$, its matrix factors $\mathbf{U}_1$, $\mathbf{U}_2$ and $\mathbf{U}_3$ can be computed as the left singular vectors of its matrix unfoldings [11]. Then, we can rewrite Eq. (1) as

$$\max_{\mathbf{U}} \sum_{i=1}^{K} ||\mathbf{U}^T \mathbf{S}_N^{(i)} \mathbf{U}||_F^2 = \max_{\mathbf{U}} ||\mathcal{C} \times_1 \mathbf{U}_1^T \times_2 \mathbf{U}_2^T \times_3 \mathbf{U}_3^T||_F^2, \text{ s.t. } \mathbf{U}_i^T\mathbf{U}_i = \mathbf{I}\ \forall i. \tag{2}$$

A truncated version of this formulation consists in considering [12]

$$\max_{\mathbf{U}} \sum_{i=1}^{K} ||\mathbf{U}^T \mathbf{S}_N^{(i)} \mathbf{U}||_F^2 = \max_{\mathbf{U}} ||\mathcal{C} \times_1 \mathbf{U}^T \times_2 \mathbf{U}^T \times_3 \mathbf{I}||_F^2, \text{ s.t. } \mathbf{U}^T\mathbf{U} = \mathbf{I}. \tag{3}$$

This truncated MLSVD obtained by truncating the decomposition on the M dominant higher-order singular vectors gives in practice a good approximation of the given tensor [11]. Consequently, we take the columns of $\mathbf{U}$ to be the dominant 1-mode singular vectors that are equal to the dominant left M singular vectors of $\mathbf{X}_{(1)}$. The truncated MLSVD obtained does not minimize exactly Eq. (1) but is easier to implement and much faster. The principle of the whole algorithm is presented in Algorithm 1.

Algorithm 1 Multi-View Clustering($\mathbf{S}^{(1)}, \mathbf{S}^{(2)}, ..., \mathbf{S}^{(K)}, M$)

1: Build a similarity tensor $\mathcal{X}$ from $\{\mathbf{S}_N^{(1)}, \mathbf{S}_N^{(2)}, \mathbf{S}_N^{(3)}\}$
2: Obtain the unfolding matrix $\mathbf{X}_{(1)}$
3: Compute $\mathbf{U}$ from the subspace spanned by the dominant left M singular vectors of $\mathbf{X}_{(1)}$
4: Normalize the rows $(u_i)_{i=1,...,N}$ of $\mathbf{U}$ to unit length
5: Cluster the points $(u_i) \in \mathbb{R}^M$ with the k-means algorithm into k clusters

3 Results

Figure 3 presents the obtained classification on two equine tendons (healthy and injured). The number of final classes is fixed to 4. Each tile is surrounded by a colored square that shows the class this tile belongs to. One tile of each class is highlighted in details on the right of each tendon slide. One can see that the classification, even fully unsupervised, performs well. Indeed, the different classes contain tiles that exhibit similar visual histological criteria in terms of cell repartition and texture. For the healthy tendon, most of the tiles are classified into only one class, assessing the fact that the tissue is almost the same everywhere. For the injured tendon, one can see a concentration of tiles (colored in magenta) that distinguish a specific area of lesion (confirmed by the experts) from the rest of the slide.

4 Conclusion

This work has shown that an automatic analysis of whole slide images of equine tendinopathy is possible and can be very effective as a tool for treatment quality assessment. Indeed our method is able to identify the different similar zones and can be used to monitor the lesion regression. The system can however be further enhanced. First, we plan to incorporate other visual histological criteria such as fiber crimp. It is important to note that the incorporation of new feature views of the data can be easily performed by simply adding a new similarity matrix to the tensor-based spectral clustering. Second, we plan to replace the k-means clustering by a supervised classification with the help of a ground truth classification of tiles from several images.

References

1. McIlwraith, C.: Diseases of joints, tendons, ligaments and related structures. In Stashak, T., ed.: Adams' Lameness in Horses. 4th edn. Lippincott Williams and Wilkins (2002) 339–485
2. Bloom, W., Fawcett, D.: A textbook of histology. 10th edn. W.B. Saunders (1975)
3. Denoix, J., Audigié, F., Hinchcliff, K., Kaneps, A., Geor, R.: Imaging of the musculoskeletal system in horses. Equine sports medicine and surgery: basic and clinical sciences of the equine athlete (2004) 161–187
4. Crovace, A., Lacitignola, L., Rossi, G., Francioso, E.: Histological and immunohistochemical evaluation of autologous cultured bone marrow mesenchymal stem cells and bone marrow mononucleated cells in collagenase-induced tendinitis of equine superficial digital flexor tendon. Vet Med Int. (2010)

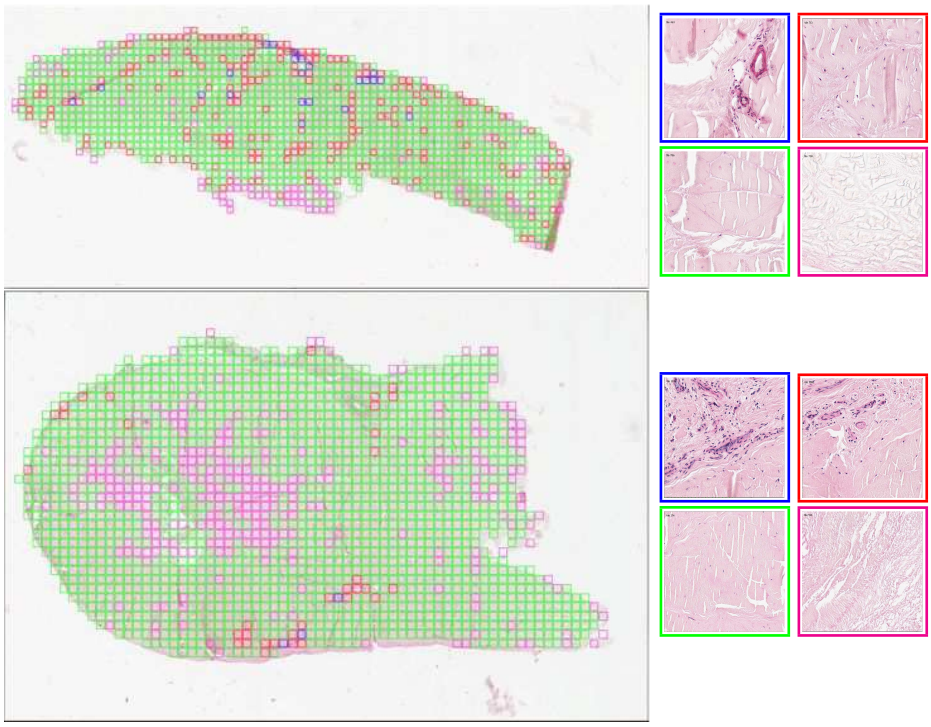

Fig. 3. Classification result with $k = 4$ on healthy (top) and injured (bottom) equine tendons with, on the right, one typical tile of each class. The color around each tile corresponds to one extracted class.

5. Roullier, V., Lézoray, O., Ta, V., Elmoataz, A.: Multi-resolution graph-based analysis of histopathological whole slide images: application to mitotic cell extraction and visualization. Computerized Medical Imaging and Graphics **35** (2011) 603–615
6. Ruifrok, A., Johnston, D.: Quantification of histochemical staining by color deconvolution. Analytical and Quantitative Cytology and Histology **23** (2001) 291–299
7. Ojala, T., Pietikäinen, M., Mäenpää, T.: Multiresolution gray-scale and rotation invariant texture classification with local binary patterns. IEEE Trans. Pattern Anal. Mach. Intell. **24** (2002) 971–987
8. Doyle, S., Agner, S., Madabhushi, A., Feldman, M., Tomaszewski, J.: Automated grading of breast cancer histopathology using spectral clustering with textural and architectural image features. In: Biomedical Imaging: From Nano to Macro, 5th IEEE International Symposium on. (2008) 496–499
9. Vanegas, M., Bloch, I., Inglada, J.: Searching aligned groups of objects with fuzzy criteria. Computational Intelligence for Knowledge-Based Systems Design (2010) 605–613
10. Rüping, S., Scheffer, T., eds.: Learning with multiple views, ICML Workshop on Learning with Multiple Views (2005)
11. DeLathauwer, L., DeMoor, B., Vandewalle, J.: A multilinear singular value decomposition. SIAM J. Matrix Anal. Appl. **21** (2000) 1253–1278
12. Liu, X.: Learning from multi-view data: clustering algorithm and text mining application. PhD thesis, Katholieke Universiteit Leuven (2011)